ISBN: 978-3-95450-247-9 ISSN: 2673-5490 doi: 10.18429/JACoW-IPAC2024-TUPC72

IMPROVEMENTS OF THE SPS SLOW EXTRACTION ELECTROSTATIC SEPTUM

F. Lackner*, F. Pirozzi, N. Roudaut[1], A. Prost, L. Jorat, K. Kawa[2]
H. Vincke, B. Balhan, J. Borburgh, M. Faser, CERN, Geneva, Switzerland
[1] also at University of Technology Belfort-Montbeliard, Sevenans, France
[2] also at AGH University of Krakow, Poland

Abstract

The impact of high-flux protons on the inherent beam loss in the slow extraction straight from SPS towards the North Area has been recently discussed and potential improvements have been proposed. These solutions are mainly aiming to reduce the high component activation and related reduction of lifetime, as well as observed non-straightness in the anode body. Recent studies have allowed to demonstrate feasibility of replacing the currently installed stainless steel tank, flanges, and anode body by a low-Z based material alternative. The design iteration and material choice has led to the current fabrication of a reduced length prototype, demonstrating mechanical, electrical, as well as the vacuum related performance. The mass reduction of the anode body has been optimized using numerical simulation, considering mechanical and thermal constraints. The paper presents the challenges related to the development of a low-Z material based vacuum tank and anode solution.

INTRODUCTION

The SPS slow extraction system towards the North Area (FT) physics programme is located in the Long Straight Section (LSS) 2 and consists of five electrostatic septa (ZS), upstream line of magnetic septa (MST, MSE). Each ZS vacuum tank has a length of 3.1 meters and a diameter of 580 mm. The anode body is supported inside the tank and equipped with 2080 W-Re wires of 60 µm diameter on the first and second ZS anode, and 100 µm diameter on ZS anodes three to five. The wires separate low and high electric field regions.

Figure 1 provides a view of the vacuum tank and the inner anode and supporting system.

Figure 1: Electrostatic septum inside vacuum tank.

The mechanical engineering challenge of these devices is given by the required straightness of the anode to wire interface, specified to 20 µm over the entire anode length, reducing the unavoidable scattering of the particle beam. Increased beam-loss during the recent operations have triggered a stringent analysis, revealing an observed increase of anode straightness to larger than 500 µm [1–3]. A root cause analysis has shown several potential sources for the observed anomaly. Small extracted samples from the anode body allowed to perform an X-ray diffraction tomography of the FeNi36, confirming internal stresses. A small sample dilatometry also indicated a higher coefficient of thermal expansion in comparison to a reference FeNi36 sample. Since the devices have been in operation since 40 years, these results could not be compared to the reference material from that period. Therefore, the results can only indicate potential plastic deformation impact due to irradiation or thermal, and mechanical constraints throughout a commissioning phase or operation [4–6].

ANODE DEVELOPMENT

The current anode body is made of either invar (FeNi36) or stainless steel (SS304L) material. With its mass of 300 kg there is a significant impact on the overall system activation cool-down after operation. Changing the anode mass would therefore be beneficial, further reducing the radiation cool-down prior to any intervention for maintenance. Two main paths are currently being investigated. In a first iteration a topology optimization, without considering a change of material, has been performed. This optimization has shown a total anode mass reduction of 35%. However, the reduction of mass also impacts the structural stiffness and therefore the straightness of the critical anode to wire interface. This aspect becomes critical in the second iteration, where low-Z materials have been considered, allowing to reduce the anode mass and therefore the activation [7]. The material change towards the Al5083 offers a factor two reduction of activation after one week of cool-down when comparing to the current SS304L material. Numerical simulations based on Al5083 or Ti6Al4V has been launched, indicating the impact on the straightness. Table 1 is summarizing the mass reduction and impact on the straightness. The topology optimization based on the AL5083 alloy shows a reduction factor of three in mass when compared to SS304L, with a minor increased straightness to 22 µm. A proposal to modify the anode support system towards the optimized Bessel points further improves straightness by factor two, while also reducing the vertical deformation by 2 mm. Due to the mentioned manufacturing and functional constraints, the anode's rear section optimization has shown the highest potential for the overall mass optimization. The primary target value for

* Friedrich.Lackner@cern.ch

ISBN: 978-3-95450-247-9 ISSN: 2673-5490 doi: 10.18429/JACoW-IPAC2024-TUPC72

this numerical optimization was kept at 35% volume reduction with the maximization of stiffness as an optimization objective. A further step is currently ongoing by verifying the thermal impact which remains critical when optimizing for the specified anode straightness. The study includes an active cooling scenario to reduce the critical temperature gradients which will lead to local straightness variations.

Table 1: Anode Mass And Straightness, Numerical Results

Material	Mass (kg)	Reduction rate (%)	Straightness (µm)
FeNi36	291	Reference	12
SS304L	284	2	7
Al5083	96	67	22
Ti6Al4V	157	46	12

Figure 2 shows FEA optimized rear structure of the anode. All relevant features in terms of functionality (interface for motorization, ion traps, high voltage, wire tension system) have been preserved and geometrically not modified. The final design is currently adapted to the preferred manufacturing process.

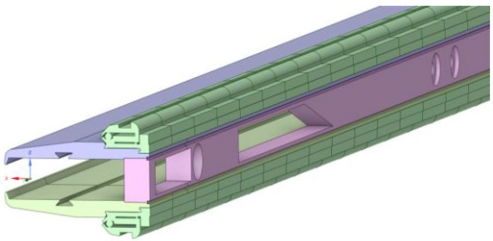

Figure 2: Structural optimization of the anode.

LOW-Z VACUUM TANK DEVELOPMENT

As described above, low-density materials can reduce the radiation hazard of exposed equipment. The development of a Low-Z vacuum tank is considered of primary interest in terms of reducing personnel dose rate during hands-on maintenance. The project will underline the feasibility for further applications [8, 9].

Material Choice

Material alternatives to stainless-steel have been investigated using a Figure of Merit [10] which combines the material transparency to the beam particle (related to material density) and the mechanical stability (related to Young's Modulus) as the main failure mode of a vacuum chamber is the radial buckling under the internal and external vessel pressure gradient of 1 bar. According to Table 2, Beryllium is identified as best alternative but it has significant drawback such as toxicity. Structural Composites like carbon fiber composites (CFC) represent an attractive solution but the current State of Art [11] excludes the possibility of having an CFC tank in the near future. Aluminium is preferred over Titanium for better transparency, faster radiation cool-down and less procurement and manufacturing costs.

Table 2: Material Classification Based On FoM

Material	Be	CFC	Al	Ti	St. Steel
FoM	2.3	1.58	0.37	0.18	0.1

Low-Z Tank Concept

The current ZS tank layout (position of lateral and front/back ports), shown in Fig. 3, will be preserved to keep compatibility with installed ZS equipment. The main vessel body (3 m x ϕ 586 mm cylinder) will be made of EN AW 5083-H111 alloy since recommended for ultra-high vacuum applications, combining mechanical strength, high corrosion resistance, weldability, and extrudability (lateral ports).

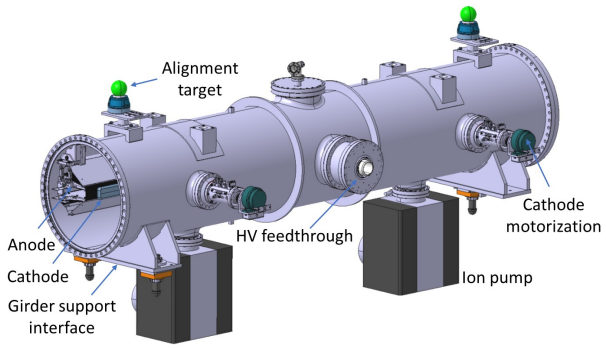

Figure 3: ZS tank layout.

The ConFlat (CF) flange system will be used for all ports to withstand a vacuum level of 10^{-9} mbar. A bimetallic transition, created via explosive bonding technology, will allow to create a composite material with a multi-layer configuration (Fig. 4). The layer consist of Al5083-H111 (20 mm), welded to the Al5083-H111 vessel body, a layer of SS316LN (5 mm) for the ConFlat knife-edge in order to benefit of a higher mechanical strength and preserve the integrity of the sealing knife edge. As Al5083 and SS316LN have poor metallurgical compatibility, a required transition is created using an inter-layer of 5 mm made by Titanium grade 1 and pure Aluminium. This will create a high-quality metallurgical bond between the four layers, profiting from the mechanical properties of each interface.

Analytical and Numerical Computation

The design process requires the demonstration of the mechanical stability under atmospheric pressure. The buckling strength depends on the Young's Modulus, which is reduced by factor 3 for the chosen Al alloy. Equation (1) provides the linear buckling limit pressure (P_{LB} in MPa) [12]. Fixing the tank mean radius (R) to 293 mm, the reduction of the modulus (E) requires compensation via an increased vessel thickness (t) from 6 mm to 10 mm as shown in Table 3.

ISBN: 978-3-95450-247-9 ISSN: 2673-5490 doi: 10.18429/JACoW-IPAC2024-TUPC72

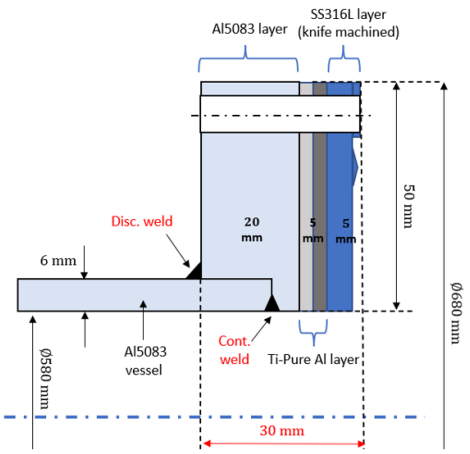

Figure 4: Schematic of ConFlat bimetallic flange concept.

$$P_{LB} = 0.28E(t/R)^3 \quad (1)$$

Table 3: Buckling Limit Pressure Comparison

Material	E [MPa]	t [mm]	P_{LB} [MPa]
SS	200000	6	0.88 (8.8 bar)
Al	70000	10	0.77 (7.7 bar)

The design criterion for linear buckling requires a Safety Factor (SF) of at least 4 ($P_{LB} \geq 4$ [13]). As shown in Table 3, the Al tank with t=10 mm provides a SF=7.7 against the 1 bar external pressure, therefore the thickness could be further reduced, optimizing the mass. However, Eq. (1) refers to a basic model, assuming a long cylindrical thin-walled ideal geometry. This provides only a rough estimation of the critical pressure, which is impacted by other parameters but not accounted in the theoretical model. These parameters are given by the implementation of lateral ports, manufacturing imperfections (cylindrical tolerances), and structural load (vacuum pumps and ZS equipment). These can reduce the effective buckling strength by up to 50% concerning a theoretical model. Equally spaced reinforcement rings can be added to compensate for these reduction factors. A mass optimization process [14] allowed to find the minimum vessel thickness and to meet the requirements $P_{LB} \geq 4$. The standard EN 13445-3 (Chapter 8) is applied to several combinations of reinforcement quantities to compute the related buckling limit pressure depending on the vessel thickness. This allows the identification of suitable solutions and to exclude combinations with a too-high or too-low safety factor. The selected combinations are shown in Table 4.

A non-linear buckling numerical model has been built to analyze the combinations selected in Table 4, taking into account the effect of the real tank geometry and the deviation from a perfect cylindrical shape (manufacturing tolerances). These are implemented using an Ansys Parametric Design Language (APDL) script, developed at CERN. The

Table 4: Buckling Limit Pressure [MPa] For Selected Thickness-Number Of Stiffeners Combinations

N of stiffners	4 mm	5 mm	6 mm	8 mm
0	x	x	x	0.67
2	x	0.66	1.07	x
4	0.65	1.14	x	x
6	0.94	x	x	x

numerical model and its critical deformation prior non-linear buckling is shown in Fig. 5.

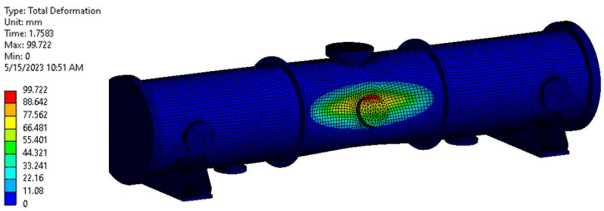

Figure 5: Critical deformation of ZS tank for the non-linear buckling analysis.

The final solution of a 6 mm wall thickness vessel with 2 equally spaced reinforcements offer a SF of 4.8. This factor is considering a cylindrical tolerance of 6 mm and a mass reduction by a factor 3 (300 Kg vs 100 Kg) due to the Al5083 alloy. A reduced 1 m long prototype is currently in production and will allow to validate all manufacturing steps including the critical welding of the bi-metal flange system. Furthermore, it will show feasibility concerning material choice and demonstrate the mechanical, electrical, as well as the vacuum related performance.

CONCLUSION AND OUTLOOK

The low-Z ZS project aims to reduce the radiation hazard in the SPS slow extraction towards the North Area. A material change to Al5083-H111 for the vacuum tank and anode body will reduce this impact by a factor of 4 after a one week system cool-down. The tank design has been preserved and was optimized for increased buckling safety of factor 4.8 for a 6 mm vessel thickness, this has been achieved by using available standards and numerical modeling. Currently, a 1 m long vacuum tank is fabricated to study all critical manufacturing and operational parameters. The anode body has been mass-optimized based on the Al5083, the impact on the mass and straightness have been discussed. The specified straightness of 20 µm requires a thermal analysis, currently ongoing, to validate beam-induced heating and its impact on the straightness parameters. The overall anode straightness will be verified by an automated and recently implemented optical metrology. After successful commissioning first practical tests are in progress which will be reported at later stage. The implementation of a first low-Z ZS is foreseen during Long Shutdown 3.

ISBN: 978-3-95450-247-9 ISSN: 2673-5490 doi: 10.18429/JACoW-IPAC2024-TUPC72

REFERENCES

[1] M.A. Fraser *et al.*, "First measurements of SPS slow-extraction inefficiency", presented at the Machine Studies Working Group meeting, CERN 2016. https://indico.cern.ch/event/559108/

[2] M. A. Fraser *et al.*, "Modeling the Radioactivity Induced by Slow-Extraction Losses in the CERN SPS", in *Proc. IPAC'17*, Copenhagen, Denmark, May 2017, pp. 1897–1900. doi:10.18429/JACoW-IPAC2017-TUPIK086

[3] M. A. Fraser *et al.*, "SPS Slow Extraction Losses and Activation: Update on Recent Improvements", in *Proc. IPAC'19*, Melbourne, Australia, May 2019, pp. 2391–2394. doi:10.18429/JACoW-IPAC2019-WEPMP031

[4] A. Golutvin *et al.*, "A Facility to Search for Hidden Particles (SHiP) at the CERN SPS", CERN, Geneva, Switzerland, Rep. CERN-SPSC-2015-016 (SPSC-P-350), 2015.

[5] R. Jacobsson *et al.*, "A new Experiment to Search for Hidden Particles (SHiP) at the SPS North Area", CERN, Geneva, Switzerland, Rep. CERN EN-DH-2014-007 EDMS 1369559, 2015.

[6] B. Balhan *et al.*, "Improvement to the CERN SPS electrostatic septa ion traps", *27th International Symposium on Discharges and Electrical Insulation in Vacuum*, Suzhou, China 2016, pp. 1-4. doi:10.1109/DEIV.2016.7764034

[7] H. Vincke and C. Theis, "ActiWiz - optimizing your nuclide inventory at proton accelerators with a computer code", *Prog. Nucl. Sci. Tech.*, vol. 4, pp. 228–232, Apr. 2014. doi:10.15669/pnst.4.228

[8] D. Björkman *et al.*, "Progress on the LSS2 FLUKA model", presented at SPS Losses and Activation Working Group meeting, CERN, Geneva, Switzerland, vol. 5, Apr. 2017.

[9] D. Björkman *et al.*,"Alternative Material Choices to Reduce Activation of Extraction Equipment", in *Proc. IPAC'19*, Melbourne, Australia, May 2019, pp. 2363–2366. doi:10.18429/JACoW-IPAC2019-WEPMP024

[10] C. Garion, "New Materials for Vacuum Chamber in High Energy Physics", *World Journal of Mechanics*, vol. 4, pp. 71-78, Mar. 2014. doi:10.4236/wjm.2014.43008

[11] G. Engelmann *et al.*, "Vacuum chambers in composite material", *Journal of Vacuum Science & Technology*, vol. 5, pp. 2337-2341, Jul. 1987. doi:10.1116/1.574447

[12] C. Hauviller, "Design rules for vacuum chambers", CERN, Geneva, Switzerland, Rep. CERN-CDS NOTE, 2007.

[13] I.R. Collins, "Mechanical and Vacuum SSubility Design Criteria for the LHC Experimental Vacuum Chambers", CERN, Geneva, Switzerland, Rep. LHC Project Report 205, 1998.

[14] F. Pirozzi, "Design optimization of aluminium vessel for ZS extraction equipment via non-linear buckling analysis", CERN, Geneva, Switzerland, Rep. EDMS 2896062, CERN 2023.